

Article

## Deformation of Honeycomb with Finite Boundary Subjected to Uniaxial Compression

Dai-Heng Chen <sup>1</sup> and Kuniharu Ushijima <sup>2,\*</sup>

<sup>1</sup> Department of Mechanical Engineering, Tokyo University of Science, 6-3-1 Nijjuku, Katsushika-ku, Tokyo 1258585, Japan; E-Mail: chendh3124@gmail.com

<sup>2</sup> Department of Mechanical Engineering, Kyushu Sangyo University, 2-3-1 Matsukadai, Higashi-ku, Fukuoka 8138503, Japan

\* Author to whom correspondence should be addressed; E-Mail: kuniharu@ip.kyusan-u.ac.jp; Tel.: +81-92-673-5605; Fax: +81-92-673-5090.

Received: 9 October 2013; in revised form: 12 November 2013 / Accepted: 19 November 2013 /

Published: 25 November 2013

---

**Abstract:** In this paper, the crushing behavior of hexagonal honeycomb structures with finite boundaries (finite width and height) subjected to in-plane uniaxial compressive loading is studied based on the nonlinear finite element analysis. It is found that stress-strain responses for the honeycombs with finite boundaries can be classified into two types: Type I and Type II. Such a characteristic is affected by the wall thickness, the work-hardening coefficient and the yield stress for the honeycombs. Furthermore, a transition from the symmetric to asymmetric deformation mode can be observed in Type I, and these deformed cells were localized in a horizontal layer. However, for the case of Type II response, the symmetric and asymmetric deformation modes can be observed simultaneously, and the region of the asymmetric mode was formed by the cell layer along the diagonal direction. As a result, the shear deformation behavior was developed along that direction. Moreover, the effect of work-hardening on the deformation behavior for the honeycombs with finite boundaries can be explained from that for infinite honeycombs.

**Keywords:** honeycomb; hexagonal cell; buckling; finite element method; work-hardening; deformation mode; uniaxial compression

---

## 1. Introduction

Cellular structures, like honeycombs, have been widely used as energy absorbing devices for various engineering applications. Various buckling modes that occur under in-plane compressive loads have been the subject of extensive analytical and experimental research [1–23].

For example, Prakash *et al.* [7] studied the effect of end constraints on the formation of a shear band in a regular hexagonal honeycomb under in-plane and out-of-plane compressive loadings. Furthermore, Wang and McDowell [16,17] theoretically studied the in-plane stiffness and plastic yield strength of periodic metal honeycombs. Specifically, they introduced the critical value of the cell's thickness to length ratio,  $t/l$ , to distinguish the occurrence of elastic buckling and plastic yielding observed in the honeycomb. On the contrary, Klintworth [1] has classified these buckling modes into six (mode I–VI), which is based on the deformation behavior of one hexagonal cell in a honeycomb structure. They investigated the effects of the cell's geometries and loading conditions on the occurrence of elastic buckling. Furthermore, they proposed theoretical equations for describing the compressive stress-strain relationship after buckling. Furthermore, these buckling modes I–VI proposed by Klintworth [1] can be roughly divided into two types (symmetric and asymmetric types). Each mode can be distinguished by the movements of the vertical and inclined cell. Klintworth [1] has reported that the in-plane crushing deformation of a honeycomb structure is always asymmetric under uniaxial compression in the same direction along the vertical wall of the hexagonal cell.

On the other hand, Karagiozova and Yu [15] studied the plastic deformation mode of an infinite block of honeycomb structures with relatively large wall thickness to length ratio  $t/l$  under in-plane biaxial compression. Based on their results, the following fundamental modes of plastic buckling were identified: mode  $C$  for symmetric deformation, mode  $S$  for asymmetric deformation and mode  $F$  for flower-shaped deformation. When the stress ratio,  $\sigma_y/\sigma_x$  (the  $y$ -axis lies along the vertical cell wall), is less than one, the deformation enters mode  $C$ . When the ratio  $\sigma_y/\sigma_x = 1$ , the deformation enters mode  $F$ , and when  $\sigma_y/\sigma_x > 1$ , the deformation enters mode  $S$ . Therefore, as in the case of the work by Klintworth [1], the axial crushing deformation of a honeycomb structure is already in an asymmetric type for uniaxial compression in a direction parallel to the vertical wall of a hexagonal cell.

However, from the experimental investigations for honeycombs under uniaxial compression discussed by Papka and Kyriakides [6] and Klintworth and Stronge [2,3], these buckling deformations are initially in a symmetric mode, but then changed to an asymmetric mode. The theoretical research discussed above provides no explanation for this phenomenon. The reason for this discrepancy is that in their theoretical research, each material was assumed to be a perfect plastic body with no work-hardening, and the object of their analysis was taken as an infinite honeycomb block by applying periodic boundary conditions. Therefore, in order to describe the crushing behavior of the actual honeycomb structure more accurately, it is necessary to consider the influence of finite measurements (width and height), as well as the work-hardening characteristic of the material.

In the present research, the honeycomb structure with finite boundaries (that is, finite width and height) is studied using FE analysis. The FE model is composed of an elasto-plastic material in consideration of work-hardening. In the following, the honeycomb with finite boundaries is referred to as a finite honeycomb, and in contrast, the honeycomb with a large-scale width and height is referred

to as an infinite honeycomb. The effects of the material's work-hardening, the honeycomb's geometry and the boundary conditions on the load-deformation response are investigated systematically.

## 2. Method for Numerical Analysis

In this work, the nonlinear commercial FE analysis code, MSC.Marc, is used to simulate the elasto-plastic crushing behavior of the finite honeycomb structures. The validity of our FE analysis has already been confirmed by comparing our numerical results with the other researchers' result [6], as shown in Figure 1, in which the analyzed problem is the same as that shown in Figure 1 in the study of Papka and Kyriakides [6].

**Figure 1.** Comparison of stress-strain responses for a honeycomb investigated by Papka and Kyriakides [6].

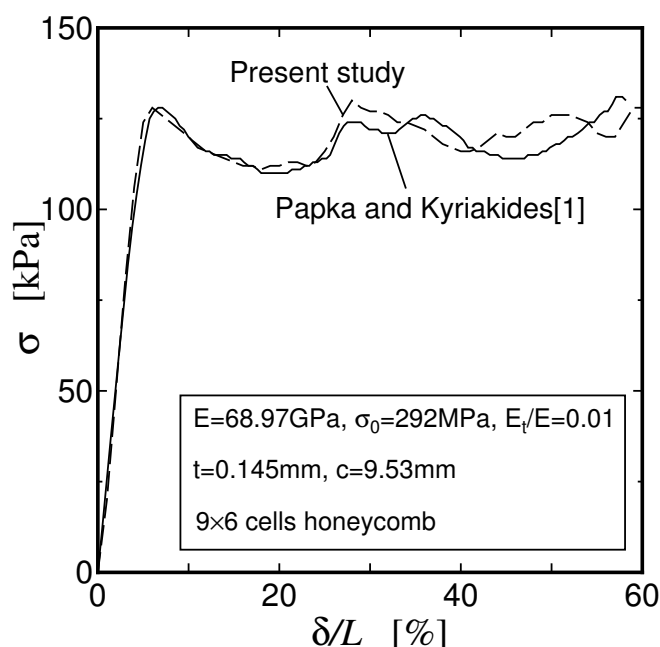
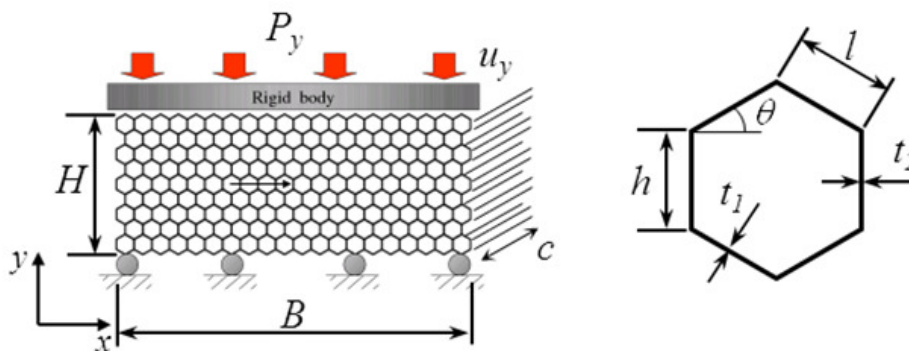


Figure 2 shows the geometry and the loading condition of the hexagonal finite honeycomb investigated in our analysis. The parameters,  $m$  and  $n$ , are introduced to represent the number of cells per row and the number of rows along the loading direction,  $y$ , respectively. For example, the honeycomb in Figure 2 has 20 columns ( $m = 20$ ) and nine rows ( $n = 9$ ). Furthermore, parameters  $t_1$  and  $l$  represent the thickness and the length of the oblique cell walls, and parameters  $t_2$  and  $h$  show the thickness and the length of the vertical cell walls, respectively. In addition, the parameters,  $P_y$  and  $u_y$ , in the Figure represent the compressive force and displacement along the  $y$ -direction, respectively. Each cell wall is modeled by four beam elements with three nodes (element number 45) in our FE analysis. This element allows transverse shear, as well as axial straining and is based on a quadratic displacement assumption on the global displacement and rotation [24]. Moreover, parameters  $B$ ,  $H$  and  $c$  represent the width, height and depth of the overall honeycomb structure, respectively, and the angle,  $\theta$ , in Figure 2 is set to  $30^\circ$ .

**Figure 2.** Analysis model of honeycomb structure with finite width and height.



As a boundary condition, the movement in the  $y$ -direction at nodes on the lower end and that in the  $x$ -direction at the center of the honeycomb are fixed in order to prevent the rigid body motion in the  $x$ -direction, and a rigid surface above the upper end is moved slowly to the honeycomb in order to compress it quasi-statically. For simplicity, the influence of friction between the honeycomb and the rigid surface is neglected, and the analysis has been conducted under a two-dimensional plane strain condition.

Moreover, as a material property, all elements in the honeycombs are assumed to be homogeneous, isotropic and elasto-plastic material and obey the von Mises yield criterion. Here, the stress-strain relationship after plastic yielding is described in the following bilinear hardening law as:

$$\sigma = \sigma_0 + \frac{E_s E_h}{(E_s - E_h)} \varepsilon^p \tag{1}$$

where  $\sigma_0$  and  $\varepsilon^p$  represent the initial yield stress and the equivalent plastic strain, and  $E_s$  and  $E_h$  represent the Young's modulus and the work-hardening coefficient of the material, respectively.

In order to avoid repetitive explanations of the parameters used in this analysis, unless described otherwise, the analyzed basic model has the following dimensions and material properties:  $l = h$ ,  $t_2 = t_1 = t$ ,  $E_s = 70.6 \text{ GPa}$ ,  $\sigma_0/E_s = 0.003$  and Poisson's ratio  $\nu_s = 0.3$ . As pointed out by Wang and McDowell [16], the slenderness ratio (namely, the cell's wall thickness to length ratio,  $t/l$ ) is one of the key factors to affect the deformation behavior for honeycombs. Specifically, if the ratio is less than  $\sqrt{12\sigma_0/(E_s\pi^2)}$ , the elastic buckling precedes the plastic yielding. In this paper, the ratio is set within the range between 0.03 to 0.20 in order to investigate the effect of plastic strain hardening on the deformation behavior. Furthermore, the normalized hardening coefficient,  $E_h/E_s$ , is changed from 0 to 0.05.

In the following section, the compressive strain,  $\varepsilon$ , and stress,  $\sigma$ , determined by the following equations are used to discuss the compressive response of honeycomb structures as:

$$\varepsilon = u_y/H \tag{2}$$

$$\sigma = P_y/(Bc) \tag{3}$$

Here, the stress at the initiation of plastic yielding for honeycombs is denoted by  $\sigma_p$  and given by [8]:

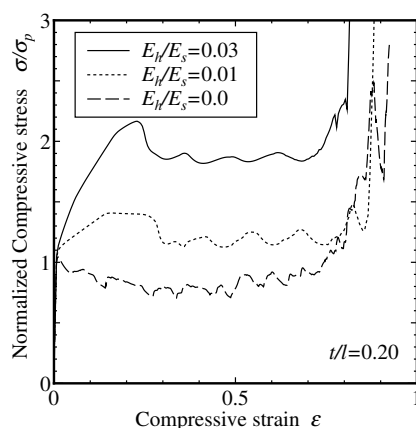
$$\sigma_p = \frac{t^2}{2l^2 \cos^2 \theta} \sigma_0 \tag{4}$$

### 3. Results and Discussion

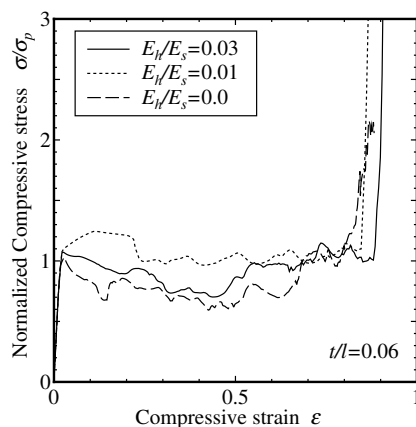
#### 3.1. Crushing Characteristics of Two Types

Figures 3 and 4 show the compressive stress-strain traces for the finite honeycombs having different cell thickness to length ratios  $t/l = 0.20$  and  $0.06$ . Here, in order to investigate the effect of the work-hardening coefficient,  $E_h$ , on the stress-strain response, three kinds of the normalized hardening coefficients,  $E_h/E_s$ , are applied in our calculations. As can be found from these Figures, the compressive stress-strain responses differ from each other and depend on their relative thickness,  $t/l$ , and the normalized hardening coefficient,  $E_h/E_s$ . Furthermore, based on the characteristics of stress-strain traces obtained by FEM, the compressive response can be categorized into two types: Type I and Type II. In order to investigate the compressive behaviors for these two types, the stress-strain responses and the corresponding deformed shapes are shown in Figures 5 and 6 as an example of Type I, where the ratios  $t/l = 0.20$  and  $E_h/E_s = 0.01$ , and those in Figures 7 and 8 as an example of Type II, where the ratios  $t/l = 0.06$  and  $E_h/E_s = 0.01$ . Furthermore, the deformed shapes of one hexagonal cell located at the center position A at stages (a), (b), (c) and (d) in Figure 5 are shown in Figure 6. Moreover, the deformed shape of cells located in positions A, B and C at stage (a) in Figure 7 are shown in Figure 8.

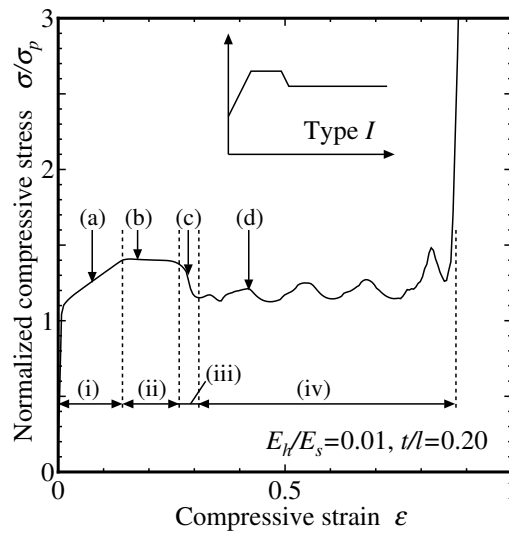
**Figure 3.** Stress-strain responses of a finite honeycomb with  $t/l = 0.20$ .



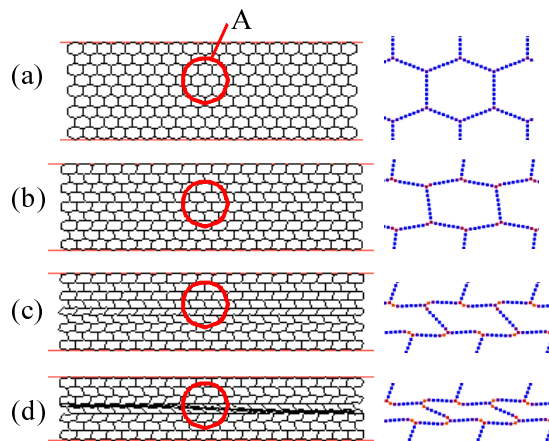
**Figure 4.** Stress-strain responses of a finite honeycomb with  $t/l = 0.06$ .



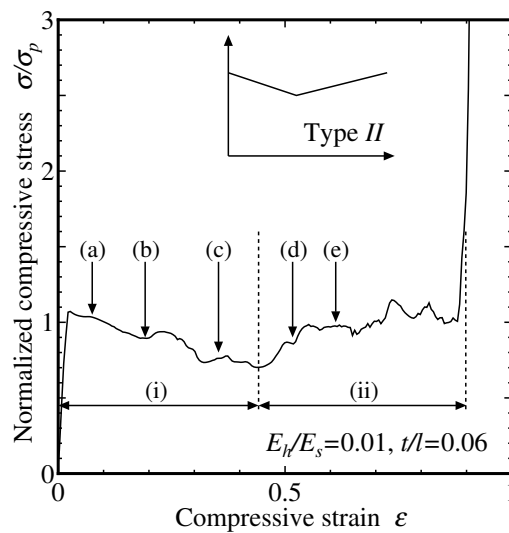
**Figure 5.** Typical stress-strain response of Type I.

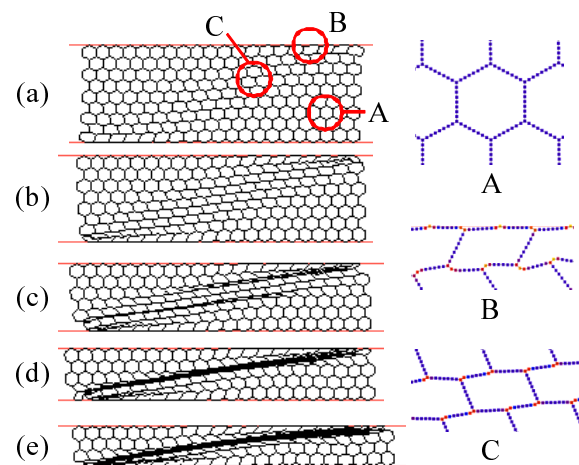


**Figure 6.** Deformation process of Type I honeycomb.



**Figure 7.** Typical stress-strain response of Type II.



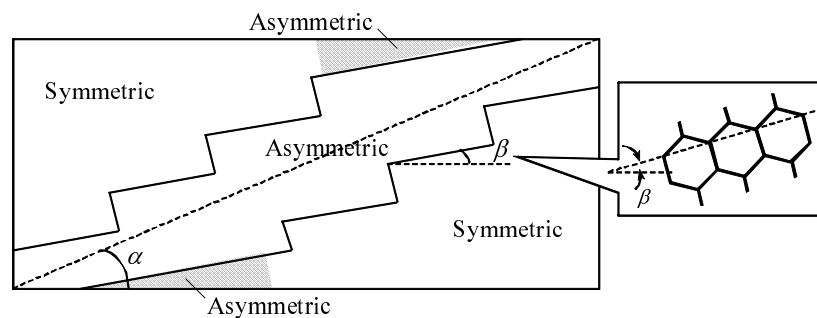
**Figure 8.** Deformation process of Type II honeycomb.

As can be seen in Figure 5, the Type I compressive response can be classified into four steps, termed (i), (ii), (iii) and (iv). In the first step, termed (i), although a small extent of the bending deformation can be seen in the vertical cell walls at the left and right ends of the structure, almost all cells deform symmetrically without any rotational deformations in the vertical cell walls, as shown in the deformation state in Figure 6(a). Furthermore, during this step, the compressive stress increases. This is what is called the “stretch-controlled” mechanism. In the second step, termed (ii), the bending deformation of the vertical cell walls at the left and right ends becomes significant. As a result, the symmetry of deformation has been lost and the deformation undergoes a transition to asymmetry with the rotational deformation in the vertical cell wall, which can be found in Figure 6(b). Since such a mode transition occurs in each cell, the stress-strain response exhibits another characteristic in comparison with that in the first step. In the third step, termed (iii), the localized deformation arises, and a large deformation is concentrated near one row in the middle. This is what is called the “bending-controlled” mechanism. Once the “bending-controlled” mechanism is generated, the following deformation behavior is governed by the local bending in the honeycomb structure. As a result, the stress drops abruptly. Then, in the final step, termed (iv), the cells in the row in which the localization was concentrated are crushed progressively, and the compressive stress rises, due to the densification. Such a localization of deformation translates immediately to the neighboring rows. Therefore, the compressive stress fluctuates with a constant period, due to the crushing of each row. This corresponds to the so-called plateau region described by Gibson and Ashby [8], and its deformation process has been already verified experimentally by Klintworth and Stronge [2,3], as well as analytically and experimentally by Papka and Kyriakides [6]. However, the transition of the deformation mode from symmetry to asymmetry has not been explained in their theoretical research for infinite honeycombs without considering the finite boundary and the work-hardening characteristic of the material.

On the other hand, as can be seen in Figure 7, the compressive response for Type II is divided into two steps. In the first step, three kinds of deformed shapes can be found, as observed for the cells at positions A, B and C in Figure 8. Specifically, the cells at position A deform symmetrically and do not undergo further deformation, while the cells at position B deform asymmetrically, as noted by Klintworth [1], with the vertical cell walls rotating in directions that differ for every row. The cells at position C also

deform asymmetrically, but the rotational directions of the vertical cell walls are the same, in contrast to the rotation for cells at position B. Hereinafter, the asymmetric modes at positions B and C are referred to as alternating asymmetry and parallel asymmetry, respectively. The Type II deformation process is regarded as the “bending-dominated” mechanism. As shown schematically in Figure 9, the cells with parallel asymmetry form prominent layers, due to the localized shear deformation along a diagonal line emanating from the angle part of the structure (in the following, these layers are referred to as the shear layers). In the vicinity of the ends of the shear layer, the cells are crushed and enter the alternating asymmetric deformation mode, and the top left and lower right angle parts in the figure that do not form shear layers are in a symmetric mode. Since the deformation is mainly concentrated into shear layers, the compressive stress decreases as the deformation progresses. However, the compressive stress fluctuates, due to the localized deformation propagating along the diagonal lines emanating from the angle parts. In Figure 9, the parameter,  $\alpha$ , denotes the angle that the diagonal line makes with the horizontal, and the parameter,  $\beta$ , denotes the angle that the sloping cell layer in the shear layer makes with the horizontal ( $\beta = 0$  at the start of deformation). It can be imagined from Figure 8 that the angle,  $\beta$ , increases and the angle,  $\alpha$ , decreases during compression. When the magnitude of these two angles coincide with each other ( $\alpha = \beta$ ), the deformation is concentrated in a single layer, and due to the densification of this layer, the deformation progresses to the second step. In the second step, since the layer of asymmetric deformation has been densified, the deformation is concentrated in the region of the symmetric mode, and the compressive stress increases.

**Figure 9.** Schematic representation of deformation in Type II honeycomb.



Based on the above results, the deformation behaviors of the finite honeycombs differ from those of infinite honeycombs in which all cells are deformed in the same manner. However, for the finite honeycombs, the deformation of cells in the vicinity of the free left and right boundaries slightly differs from those of other cells, due to the influence of the boundaries. Therefore, the small differences in the deformation would act as geometric imperfections and induce asymmetric deformation or localized deformation, as shown in Figures 6 and 8. As a result, the crushing deformation of the finite honeycomb differs from that of the infinite honeycomb, and the characteristics of the compressive stress-strain responses also differ from each other.

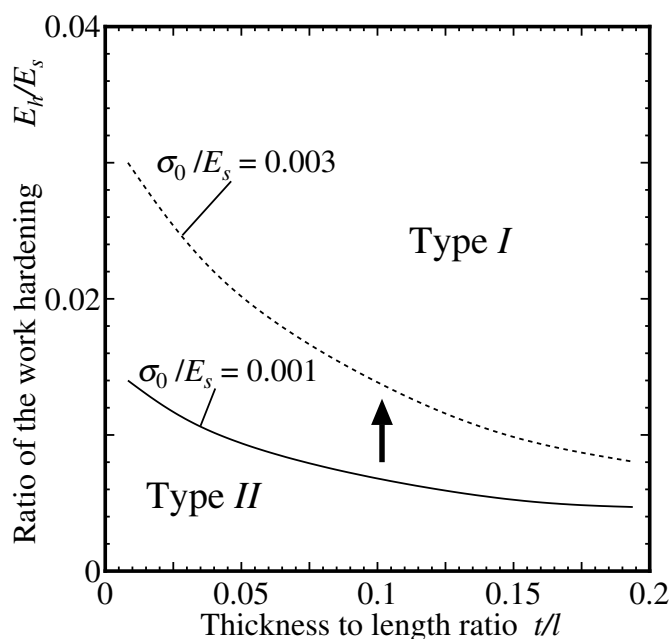
Criori *et al.* [22] investigated the failure process of honeycombs with imperfection and discussed the change of compressive stress-strain response using FE analysis. In their numerical model, the geometrical imperfection is introduced over the numerical model. On the contrary, in our numerical model, no geometrical imperfections are introduced. However, since the boundary condition for cells

near the lower or upper side is different from that for the cell around the center part of a honeycomb, some local imperfections can be created naturally by the compression process. As a result, the mode of deformation could be changed.

### 3.2. Bifurcation Line between Type I and II

Some additional numerical simulations have been conducted systematically to classify the compressive stress-strain responses for honeycombs with different combinations of thickness to length ratio  $t/l$  and normalized work-hardening coefficient  $E_h/E_s$ . As denoted previously, since the compressive response for honeycombs with finite boundaries can be categorized as Type I and II, the bifurcation line between Type I and Type II can be visualized as shown in Figure 10. It can be seen in Figure 10 that deformation Type I may occur when the work-hardening coefficient  $E_h/E_s$  and relative thickness  $t/l$  increase. In other words, Type I was generated in the case of large relative thickness  $t/l$  or a large work-hardening coefficient, while Type II was observed for small relative thickness or small work-hardening coefficient. Furthermore, by changing the yield stress ratio,  $\sigma_0/E_s$ , from 0.001 to 0.003, the bifurcation line between Type I and Type II moves upwards.

**Figure 10.** Map for deformation types I and II.



### 3.3. Effect of Honeycomb Width on the Deformation Behavior

Klintworth [1] and Karagiozova and Yu [15] have also reported that the crushing behaviors of finite honeycombs differ from those of infinite honeycombs. As for the finite honeycombs, the compressive responses are classified into Type I or Type II. In the Type I response, the transition of deformation from symmetry to asymmetry occurs. On the contrary, in the Type II response, these two deformation modes are mixed and found in the same honeycomb. In order to investigate the effects of the width of the finite honeycomb on the type of deformation, some additional numerical simulations were conducted

by changing the number of columns  $m = 10, 12, 20$  and  $40$ . Figures 11 and 12 show the stress-strain responses for various numbers of columns when the relative thickness  $t/l = 0.20$  and  $0.06$ . It can be found from Figure 10 that the former and the latter honeycombs can be categorized as Type I and II, respectively. Here, in order to distinguish these stress-strain responses, a new legend ( $m:n$ ), which specifies the numbers of columns and rows, is provided and shown in Figures 11 and 12. It can be found from Figure 12 that for Type I responses of honeycombs with the relative thickness  $t/l = 0.20$ , the deformation behaviors with different numbers of columns are basically the same at each step, (i), (ii), (iii) and (iv). However, by increasing the number of columns,  $m$ , that is, by broadening the width of the honeycomb structure, the transition to the second step can be delayed. Furthermore, since the stress-strain responses for the 20:9 model and the 40:9 model in Figure 11 are mostly overlapped, it can be anticipated that the stress-strain response would not be changed, even if the number of columns is increased further. On the contrary, as for the Type II response of the honeycombs, the distinction between steps (i) and (iv) would disappear as their width increases, especially for the 40:9 model, even though these steps can be observed for the honeycomb where the number of columns is 20 or fewer. This tendency can be explained by observing the deformed shape for the 40:9 model shown in Figure 13. It can be seen that there are some undeformed cells at the center of the honeycombs. In Figure 13, it is difficult for the generation of a shear layer along the diagonal line to occur. Finally, the localized deformation is restrained.

**Figure 11.** Stress-strain responses for various honeycomb widths under the same cell's thickness to length ratio  $t/l = 0.20$ .

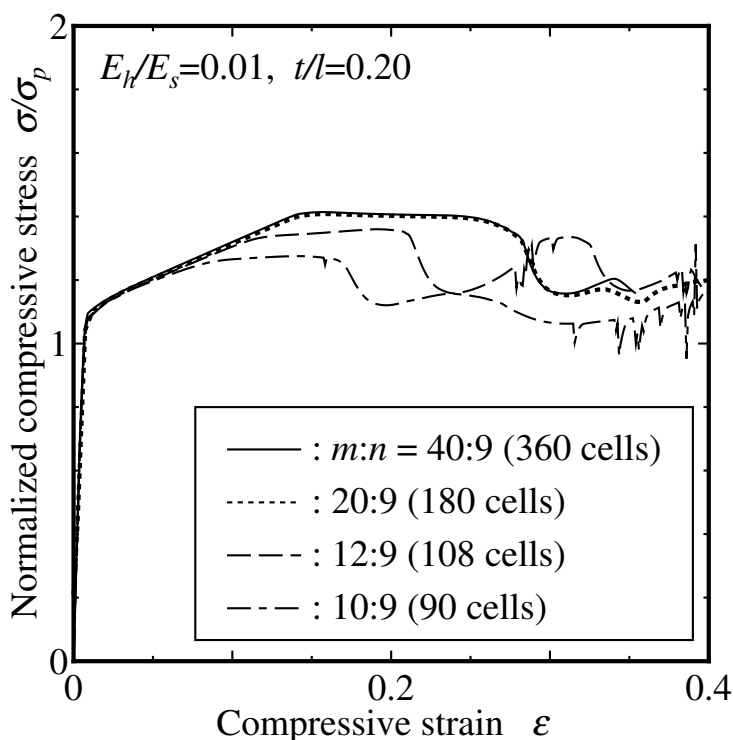


**Figure 12.** Stress-strain responses for various honeycomb widths under the same cell's thickness to length ratio  $t/l = 0.06$ .

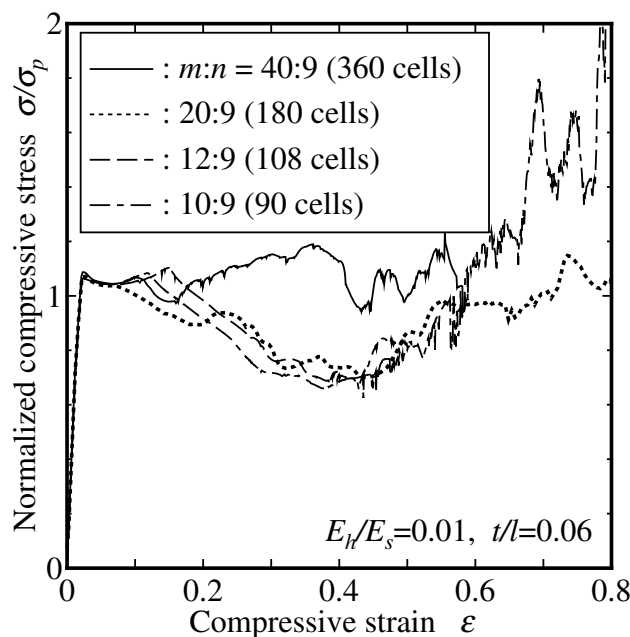
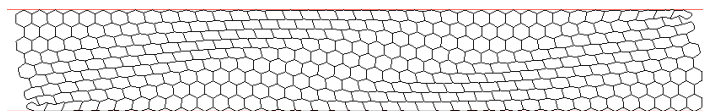


**Figure 13.** Deformed shape of Type II honeycomb with the 40:9 model.



### 3.4. Effect of Thickness of Vertical Cell Wall on the Compressive Response

In the above sections, the analyses were carried out under the condition that the vertical and the oblique cells have the same wall thickness ( $t_2 = t_1$ ). However, in a general honeycomb structure, depending on the manufacturing technique, the vertical cell wall is often twice as thick as the oblique cell wall. Here, the analysis model in which the vertical cell wall is twice as thick as the oblique cell wall, namely  $t_2 = 2t_1 = 2t$ , is referred to as the  $t$ - $t$ - $2t$  model, and the analysis model in which the thickness of the vertical cell wall is equal to that of the oblique cell wall, namely  $t_2 = t_1 = t$ , is referred to as the  $t$ - $t$ - $t$  model. The other analyses using both models are conducted and the stress-strain responses obtained are discussed in this section.

Figures 14 and 15 show representative examples of stress-strain responses obtained for finite honeycombs with the ratio  $t/l=0.20$  and  $0.06$ , respectively. It can be found from Figure 14 for Type I honeycombs that the stress-strain responses for both models coincide with each other until the second step, while the decrease in stress corresponding to the third step cannot be observed for the  $t$ - $t$ - $2t$  model. On the contrary, as seen in Figure 15 for Type II honeycombs, the first peak stresses for both models show almost the same value, but the stress values after the peak for the  $t$ - $t$ - $2t$  model behave higher than those for the  $t$ - $t$ - $t$  model. Figure 16 shows the deformation state of the  $t$ - $t$ - $2t$  model. Here, the deformed shapes at stage (d) in Figures 5 and 7 are shown in Figure 16. As can be found from Figure 16, in stage (d) for

the Type I honeycomb, the localization of deformation and the subsequent densification does not occur. On the other hand, for the Type II honeycomb, the localization occurs at the angled parts. However, due to the wall thickness of the vertical walls being doubled, the resistance against compression increases in contrast to the  $t-t-t$  model, and the localized deformation becomes difficult to develop. That is, as for the  $t-t-2t$  model, since it is more difficult to deform the vertical cell, the deformed region cannot be localized, and it is spread more widely than that for the  $t-t-t$  model. Therefore, the compressive response of the  $t-t-2t$  model can also be classified as either Type I or Type II, depending on the relative thickness,  $t/l$ . However, since the stress drop does not occur in the asymmetric deformation due to the thickness of the vertical cell walls being doubled, the localization does not occur in Type I, and the formation of the shear layer is not clear in Type II.

**Figure 14.** Stress-strain responses of Type I for the  $t-t-t$  and  $t-t-2t$  models.

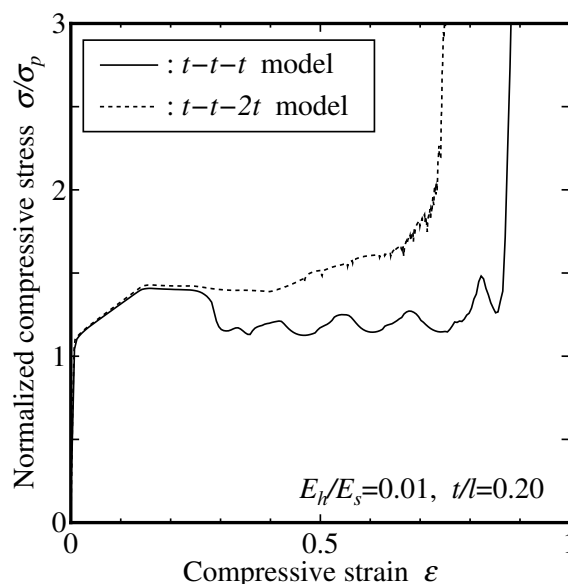


**Figure 15.** Stress-strain responses of Type II for the  $t-t-t$  and  $t-t-2t$  models.

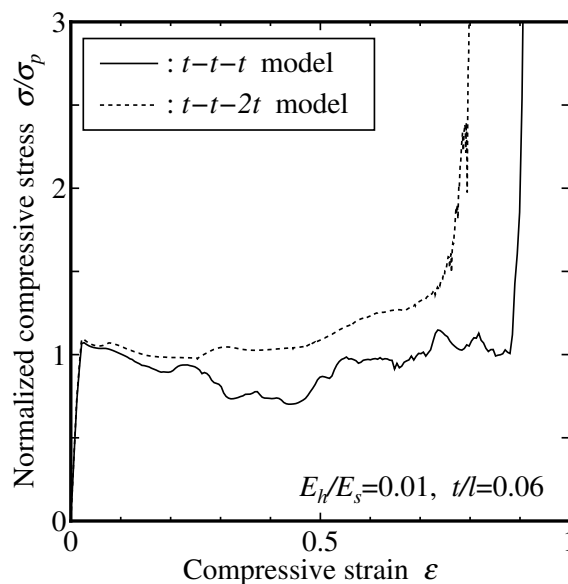
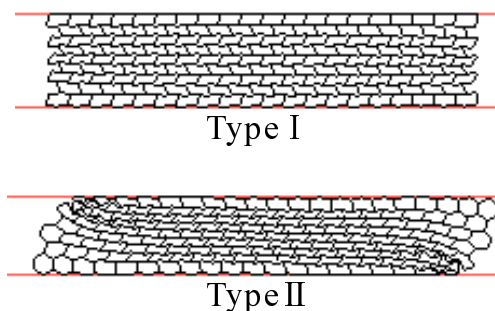


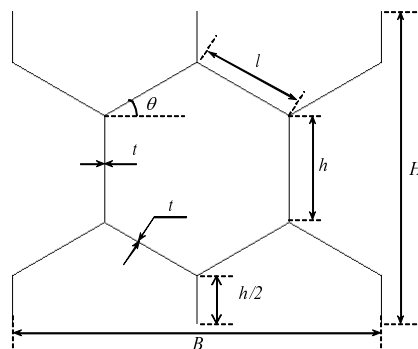
**Figure 16.** Deformed shapes of the  $t$ - $t$ - $2t$  model in process (d) shown in Figures 4 and 5.



### 3.5. Comparison of Compressive Response between Finite and Infinite Honeycombs

In order to compare the crushing behaviors of finite honeycombs with those of infinite honeycombs, the compressive response of a single cell assumed to have periodic boundary conditions in an infinite honeycomb is investigated. This single cell can be simulated using a unit model shown in Figure 17, which has been studied by Honig and Stronge [12] to investigate the validity of the theoretical values of crushing load for an infinite honeycomb (see Section 2.3 of Honig and Stronge [12] for the detailed specifications of the model).

**Figure 17.** Unit model simulating an infinite honeycomb.



Firstly, the stress-strain responses for finite honeycombs and those for infinite honeycombs are compared and shown in Figures 18 and 19. As shown previously in Figures 5 and 7, the stress-strain responses for the finite honeycombs with  $t/l = 0.20$  and  $0.06$  are classified as Type I and Type II, respectively. On the other hand, as for the infinite honeycomb, the stress-strain responses obtained by using the unit model for both symmetric and asymmetric deformations are shown in these Figures. Here, in order to generate the asymmetric deformation in the unit model, each vertical cell wall is set to have a small initial rotation angle,  $\phi_0$  (the angle that the vertical cell wall makes with  $y$ -axis), as done by Honig and Stronge [13]; a small value of  $\phi_0 = 0.01^\circ$  is used, so that the influence of  $\phi_0$  on the value of the compressive load is almost imperceptible in the Figures.

As can be seen in Figure 18, for the finite honeycombs, the compressive stress in the first step of deformation ( $\varepsilon \leq 0.1$ ) coincides with that for the infinite honeycomb. During this step, for the infinite honeycomb, the compressive stress-strain traces, due to the symmetric and asymmetric deformations, are

the same. In the second step ( $0.1 \leq \varepsilon \leq 0.3$ ), the compressive stress of the finite honeycomb is almost equal to that of the infinite honeycomb under the asymmetric deformation. During this step, for the infinite honeycomb, the compressive stress, due to the asymmetric deformation, becomes smaller than that for the finite honeycomb. This trend is based on the fact that for a finite honeycomb, the transition from the symmetric to asymmetric deformation occurs and the stress, due to symmetric deformation, is always larger than that due to asymmetric deformation. Furthermore, the asymmetric deformation gradually spreads from the central region, and some cells deformed under the symmetric mode boundary remain relatively intact in the finite honeycomb.

**Figure 18.** Stress-strain responses for finite and infinite honeycombs (Type I;  $t/l = 0.20$ ).

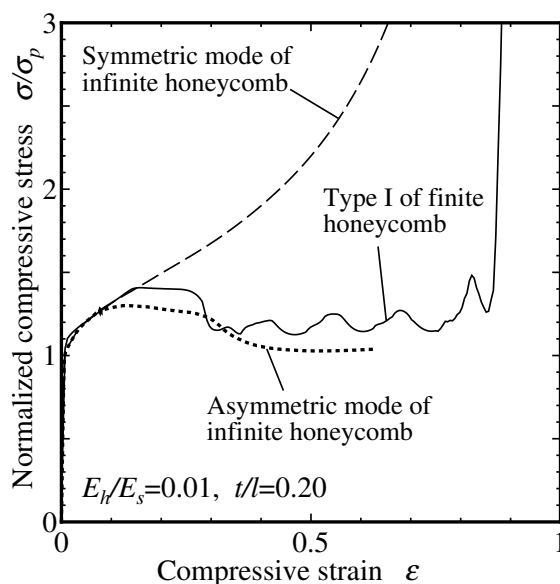
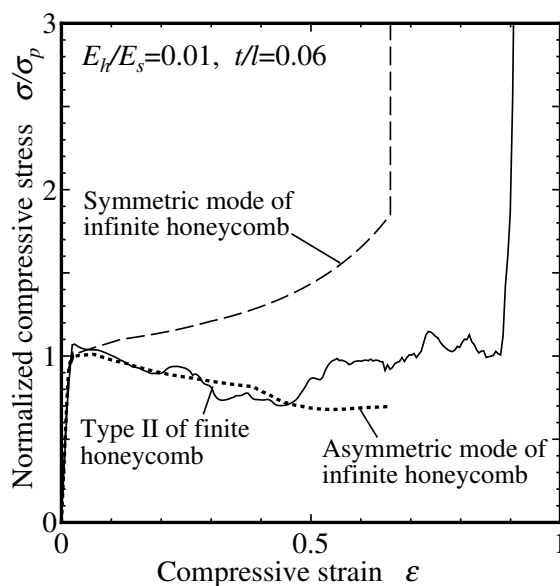


**Figure 19.** Stress-strain responses for finite and infinite honeycombs (Type II;  $t/l = 0.06$ ).



As can be understood from Figure 10, when the ratio,  $t/l$ , decreases, the obtained compressive type may be shifted from Type I to Type II. Figure 19 shows the comparison of stress-strain responses for

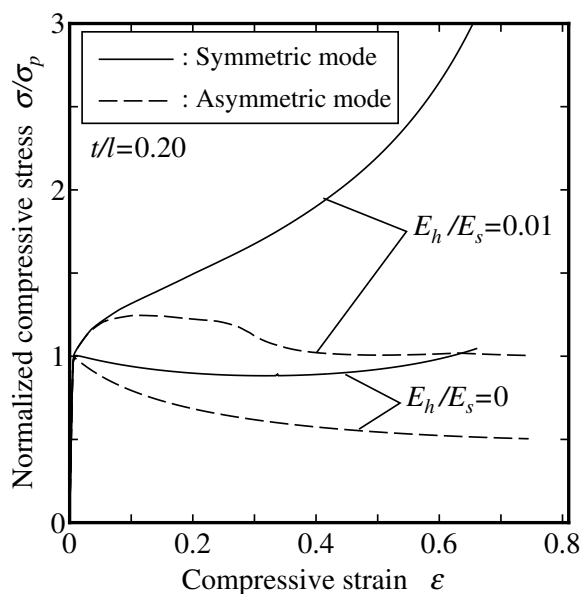
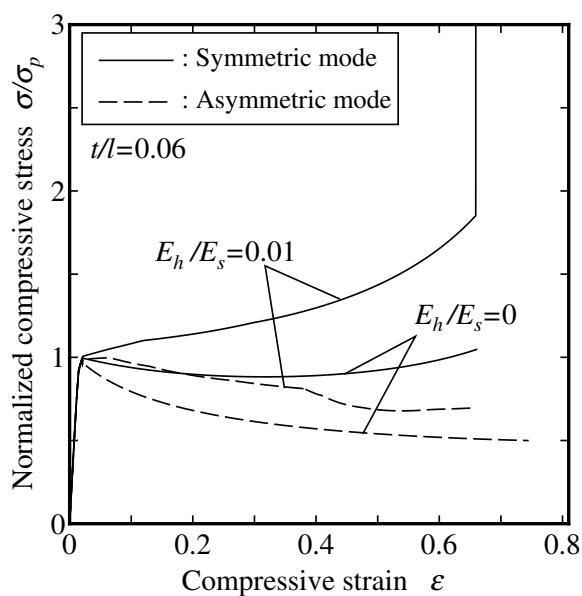
infinite and finite honeycombs under the same ratio  $t/l = 0.06$ . Here, the finite honeycomb behaves as Type II.

Furthermore, it is found from Figure 19 that for the finite honeycomb, the stress-strain response in the first step can be predicted by the stress-strain response for the asymmetric deformation mode of the infinite honeycomb. However, the strain corresponding to the minimum stress value is smaller than that for the infinite honeycomb.

As mentioned in the previous section, during the Type II deformation process of the finite honeycomb, the three modes, namely, symmetric, parallel asymmetric and alternate asymmetric deformation modes, can be observed in the honeycomb. Since the rigidity of the symmetric mode is always higher than that of the asymmetric mode, the deformation region is mainly concentrated in a shear layer on a diagonal line. Therefore, the strain corresponding to the minimum stress value is smaller, because the strain obtained by dividing the compressive deformation,  $u_y$ , by the height,  $H$ , of the finite honeycomb is smaller than the strain of cells in the shear layer.

Figures 20 and 21 show the stress-strain responses of the asymmetric and symmetric modes for infinite honeycombs with relative thicknesses of  $t/l = 0.20$  and  $t/l = 0.06$ , respectively. Here, in order to clarify the effects of work-hardening on the compressive response, additional analyses were carried out by setting two patterns of the work-hardening coefficient ratio  $E_h/E_s = 0$  and  $0.01$ . For the finite honeycomb with relative thickness  $t/l = 0.20$ , as seen from Figure 3, the stress-strain response for the honeycomb without the work-hardening ( $E_h/E_s = 0$ ) behaves as Type II. On the contrary, the response with hardening ( $E_h/E_s = 0.01$ ) behaves as Type I. This phenomenon can be understood from the response for infinite honeycombs shown in Figure 20. It is found in Figure 20 that for the honeycomb with work-hardening ( $E_h/E_s = 0.01$ ), since there exists a stage of each stress of symmetric and asymmetric modes overlapping mostly and increasing after yielding, the corresponding finite honeycomb shows a compressive stress-strain response of Type I. On the contrary, for the honeycomb without work-hardening ( $E_h/E_s = 0$ ), since the stress of the asymmetric mode decreases after yielding, the corresponding finite honeycomb shows a compressive stress-strain response of Type II. Furthermore, as can be seen from Figure 4, for the finite honeycomb with relative thickness  $t/l = 0.06$ , the variation of compressive stress is almost the same regardless of the value of hardening coefficient  $E_h/E_s$ . This can also be understood from the fact shown in Figure 21 that, even if the work-hardening coefficient is set to  $E_h/E_s = 0.01$ , the stress in the asymmetric mode of an infinite honeycomb does not increase after yielding, but is lower than that of the symmetric mode. From the results discussed above, it is found that the effects of work-hardening on the deformation for a finite honeycomb can be explained from those for an infinite honeycomb.

Finally, it can be concluded that the transition of deformation mode from symmetric to asymmetric for honeycomb structure observed by experiment can be simulated using a honeycomb model with finite boundaries and considering the material's work-hardening effect in FE analysis. Such a deformation behavior can be also explained from two results using infinite honeycomb models with and without an initial rotational imperfection.

**Figure 20.** Stress-strain responses for an infinite honeycomb with  $t/l = 0.20$ .**Figure 21.** Stress-strain responses for an infinite honeycomb with  $t/l = 0.06$ .

#### 4. Conclusions

In this study, the crushing behavior of honeycomb structures with finite width and height are studied by considering the work-hardening of the constituent material. Based on numerical results from FE analysis, the following conclusions can be found.

- (1) The stress-strain response for a finite honeycomb under uniaxial compression could be classified as Type I or Type II based on the deformation behavior. Type I was generated in the case of large relative thickness  $t/l$  or a large work-hardening coefficient, while Type II was observed for small relative thickness or a small work-hardening coefficient.

(2) A transition from the symmetric to asymmetric mode occurred in Type I. This deformation was concentrated in a horizontal layer, and the compressive stress remained nearly constant, while some fluctuation was observed. However, for Type II, the symmetric and asymmetric modes were mixed, and the asymmetric mode region was formed by the cell layer along a diagonal (shear layer), in which shear deformation is concentrated locally. Furthermore, since the deformation was mostly concentrated in this layer, the compressive stress decreased as the deformation progressed. A parallel asymmetric deformation mode that differed from the asymmetric mode proposed by Klintworth [1] was shown to exist in this shear layer.

(3) The deformations for each crushing process in Type I for finite honeycombs with a different width are basically the same. However, the transition period to the second step was found to be slowed by increasing the number of columns to a certain width. In Type II, for a certain width, the two deformation steps that were seen in the case of a small width disappeared. This was due to the increased stability of the cell with the increasing width, which limited the propagation of localized deformation. In addition, the shear layer along the diagonal was not observed.

(4) The effects of work-hardening on the deformation for a finite honeycomb can be explained by those for an infinite honeycomb.

## References

1. Klintworth, J.W. Dynamic Crushing of Cellular Solids. Ph.D. Dissertation; University of Cambridge: Cambridge, UK, 1988.
2. Klintworth, J.W.; Stronge, W. Elasto-plastic yield limits and deformation laws for transversely crushed honeycombs. *Int. J. Mech. Sci.* **1988**, *30*, 273–292.
3. Klintworth, J.W.; Stronge, W. Plane punch indentation of a ductile honeycomb. *Int. J. Mech. Sci.* **1989**, *31*, 359–378.
4. Gibson, L.J.; Ashby, M.F.; Zhang, J.; Triantafyllou, T.C. Failure surfaces for cellular materials under multiaxial loads I. Morelling. *Int. J. Mech. Sci.* **1989**, *31*, 635–663.
5. Zhang, J.; Ashby, M.F. Buckling of honeycombs under in-plane biaxial stresses. *Int. J. Mech. Sci.* **1992**, *34*, 491–509.
6. Papka, S.; Kyriakides, S. In-plane compressive response and crushing of honeycomb. *J. Mech. Phys. Solids* **1994**, *42*, 1499–1532.
7. Prakash, O.; Bichebois, P.; Brechet, Y.; Louchet, F.; Embury, D. A note on the deformation behavior of two-dimensional model cellular structures. *Philos. Mag. A* **1996**, *73*, 739–751.
8. Gibson, L.J.; Ashby, M.F. *Cellular Solids: Structure and Properties*; Cambridge University Press: Cambridge, UK, 1997.
9. Triantafyllidis, N.; Schraad, M.W. Onset of failure in aluminum honeycombs under general in-plane loading. *J. Mech. Phys. Solids* **1998**, *46*, 1080–1124.
10. Papka, S.; Kyriakides, S. Biaxial crushing of honeycombs—Part I: Experiments. *Int. J. Solids Struct.* **1999**, *36*, 4367–4396.
11. Papka, S.; Kyriakides, S. Biaxial crushing of honeycombs—Part II: Analysis. *Int. J. Solids Struct.* **1999**, *36*, 4397–4423.

12. Honig, A.; Stronge, W.J. In-plane dynamic crushing of honeycomb: Part I, Crush band initiation and wave trapping. *Int. J. Mech. Sci.* **2002**, *44*, 1665–1696.
13. Honig, A.; Stronge, W.J. In-plane dynamic crushing of honeycomb: Part II Application to impact. *Int. J. Mech. Sci.* **2002**, *44*, 1697–1714.
14. Ruan D.; Lu, G.; Wang, B.; Yu, T.X. In-plane dynamic crushing of honeycombs—A finite element study. *Int. J. Impact Eng.* **2003**, *28*, 161–182.
15. Karagiozova, D.; Yu, T.X. Plastic deformation modes of regular hexagonal honeycombs under in-plane biaxial compression. *Int. J. Mech. Sci.* **2004**, *46*, 1489–1515.
16. Wang, A.J.; McDowell, D.L. In-plane stiffness and yield strength of periodic metal honeycombs. *J. Eng. Mater. Technol.* **2004**, *126*, 137–156.
17. Wang, A.J.; McDowell, D.L. Yield surfaces of various periodic metal honeycombs at intermediate density. *Int. J. Plast.* **2005**, *21*, 285–320.
18. Li, Q.M.; Magkiriadis, I.; Harrigan, J.J. Compressive strain at the onset of densification of cellular solids. *J. Cell. Plast.* **2006**, *42*, 371–392.
19. Flores-Johnson, E.A.; Li, Q.M.; Mines, R.A.W. Degradation of elastic modulus of progressively-crushable foams in uniaxial compression. *J. Cell. Plast.* **2008**, *44*, 415–434.
20. Aktay, L.; Johnson, A.F.; Kroplin, B.H. Numerical modelling of honeycomb core crush behavior. *Eng. Fract. Mech.* **2008**, *75*, 2616–2630.
21. Cricri, G.; Perrella, M.; Cali, C. Honeycomb failure processes under in-plane loading. *Compos. Part B* **2013**, *45*, 1079–1090.
22. Cricri, G.; Luciano, R. Homogenised properties of composite materials in large deformations. *Compos. Struct.* **2013**, *103*, 9–17.
23. Hu, L.; You, F.; Yu, T. Effect of cell-wall angle on the in-plane crushing behavior of hexagonal honeycombs. *Mater. Des.* **2013**, *46*, 511–523.
24. MSC. *Marc 2012 Users Manual*; Element Library: Santa Ana, CA, USA, 2012, Volume B, pp. 288–292.